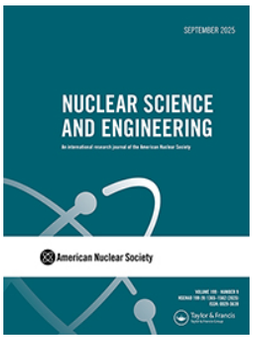

Nuclear Science and Engineering

ISSN: 0029-5639 (Print) 1943-748X (Online) Journal homepage: www.tandfonline.com/journals/unse20

Delayed Neutron Precursor Group Parameter and Spectra Generation from Fast Fission of ^{235}U in SCALE

Luke Seifert, Benjamin Betzler, William Wieselquist, Matthew Jessee, Madicken Munk & Kathryn Huff

To cite this article: Luke Seifert, Benjamin Betzler, William Wieselquist, Matthew Jessee, Madicken Munk & Kathryn Huff (26 Aug 2025): Delayed Neutron Precursor Group Parameter and Spectra Generation from Fast Fission of ^{235}U in SCALE, Nuclear Science and Engineering, DOI: 10.1080/00295639.2025.2525754

To link to this article: https://doi.org/10.1080/00295639.2025.2525754

Published online: 26 Aug 2025.

NUCLEAR SCIENCE AND ENGINEERING

DOI: https://doi.org/10.1080/00295639.2025.2525754

Delayed Neutron Precursor Group Parameter and Spectra Generation from Fast Fission of ^{235}U in SCALE

Luke Seifert,[a]* Benjamin Betzler,[a] William Wieselquist,[b] Matthew Jessee,[b] Madicken Munk,[a,c] and Kathryn Huff[a]

[a]*University of Illinois at Urbana-Champaign, Advanced Reactors and Fuel Cycles Group, 104 South Wright Street, Urbana, Illinois 61801*
[b]*Oak Ridge National Laboratory, Nuclear Energy and Fuel Cycle Division, 1 Bethel Valley Road #5200, Oak Ridge, Tennessee 37830*
[c]*Oregon State University, School of Nuclear Science and Engineering, OR211 Merryfield Hall, Corvallis, Oregon 97331*

Received February 28, 2025
Accepted for Publication June 23, 2025

Abstract — *Delayed neutron precursor (DNP) group data are important for modeling reactor dynamics. Although the data for individual DNPs have been developed over time, the DNP group data present in the Evaluated Nuclear Data Files (ENDF) have not been updated in the past 20 years. In this work, we use SCALE to recreate the Godiva experiment that was used to generate the original DNP group structure for fast fission of ^{235}U. However, each DNP is modeled using up-to-date data, and the results are then converted into a newly updated group structure. This conversion uses an iterative linear least squares solver to minimize chi-squared. The approaches used in this work also enable energy spectrum generation and uncertainty tracking. The method used in this paper for fast ^{235}U fission DNP group structure updating can be applied to different energies and fissile nuclides. Demonstration of the uncertainty tracking in reactor kinetics and dynamics simulations is shown using point reactor kinetics simulations. Results show that there are data discrepancies between the International Atomic Energy Agency database and data used in ORIGEN, which are currently being fixed. Results also show that the proposed method for group spectra generation performs well.*

Keywords — *Delayed neutron precursors, ORIGEN, SCALE, ENDF, group parameters.*

Note — *Some figures may be in color only in the electronic version.*

I. INTRODUCTION

Delayed neutron precursors (DNPs) are fission products that are beta emitting and have sufficient energy to concurrently emit a neutron. DNPs are important, as they make reactor control possible. This is because of the time delay that occurs before a delayed neutron is emitted. Thus, the time delay is based on the half-life of the beta emission. Additionally, some isotopes have sufficient

*E-mail: seifert5@illinois.edu

energy to emit multiple neutrons, each of which has different probabilities of occurring.

For many reactor kinetics and dynamics simulations, the DNPs are not all explicitly modeled. Instead, it is computationally practical to divide the DNPs into six to eight groups per fissile isotope. Each of these groups has both a half-life and a yield. The half-life of the group is based on the half-lives of the constituent DNPs in that group, while the yield is based on the amount of DNPs in that group and the average number of neutrons they emit. The differences in group half-lives and yields between different fissile nuclides are caused by fission yield differences. These yield differences affect the specific DNP concentrations, thus affecting the DNP group parameters that are calculated.

The International Atomic Energy Agency (IAEA) maintains a database of DNP data, which has updated data as recent as 2020 and was last updated in 2022.[1] Although these more recent IAEA data exist, the DNP group data used in the Evaluated Nuclear Data File (ENDF)/B-VIII.0 library have not been updated since ENDF/B-VI.8,[2] approximately 20 years ago.[3] Additionally, the spectral data have not been updated in ~30 years.[4,5] This work reconstructs the DNP groups using recent data to evaluate the group yield and decay parameters, as well as the group spectra. Comparisons are made between datasets as well as with different methods for generating the group spectra.

II. METHODS

Delayed neutron precursor group data have historically been generated either experimentally, referred to as the macroscopic approach, or computationally, referred to as the microscopic approach, by counting the delayed neutrons after irradiation.[3,5–10] For the macroscopic approach, a fissile sample is irradiated, and the delayed neutron counts are collected. For the microscopic approach, data on individual DNPs are used to simulate a delayed neutron count curve. In this work, the microscopic approach is used. Following the generation of delayed neutron counts over time, both approaches then use the same methodologies to generate DNP group parameters.

In this work, the primary difference in the generated DNP group parameters comes from the data used for the individual DNPs, as discussed in Sec. II.A. This work proposes a new method for generation of DNP group spectral fits in Sec. II.B, as the DNP group parameter fitting methodology employed in this work enables spectrum fitting as a straightforward extension. The previous approaches for generating these DNP group spectra are improved by allowing DNP group spectra to contribute to every DNP group rather than only two groups.[5,11–14] This work also shows how the DNP group parameters from different data compare when used in a point kinetics model, discussed in Sec. II.C. Section II.D discusses the specifics for the tools and models used to generate the results. The uncertainties are tracked throughout, discussed in Sec. II.E, as the more recent individual DNP data have uncertainties that can be propagated.

II.A. Group Parameter Generation

Generation of the DNP group parameters requires generation of the group yield $\bar{\nu}_{d,g}$ and group decay constant λ_g for each group. To generate these parameters, this work uses an iterative least squares approach. For a pulse irradiation with n DNP groups and m time nodes, Eqs. (2) through (5) show how the iterative least squares problem is configured for Eq. (1). The explicitly formatted pulse irradiation least squares problem is given as

$$\dot{n}_d(t) \approx \varepsilon F_s \sum_{g=1}^{n} \bar{\nu}_{d,g} \lambda_g e^{-\lambda_g t}, \tag{1}$$

which is generalizable to a format one may recall from linear algebra as

$$A\vec{x} \approx \vec{b}. \tag{2}$$

The $\bar{\nu}_{d,g}$ values are the group yield values. These represent the number of delayed neutrons per fission; when summed, they provide the total delayed neutron yield per fission. The F_s value is the total number of fission events that take place within the sample, and ε is the detector efficiency. The efficiency of the neutron detector in this work ε is set so that the Keepin et al. delayed neutron count rate, when using their group yields and decay constants, aligns with the count rate they measured.[6] The total number of delayed neutrons is calculated by integrating the delayed neutron rate curve. The number of fissions and the efficiency term are known as well. The unknowns are the decay constants for each group λ_g and the group yields $\bar{\nu}_{d,g}$. For a given set of group decay constants, the problem can be formatted as follows:

$$A = \begin{vmatrix} \lambda_1 e^{-\lambda_1 t_0} & \lambda_2 e^{-\lambda_2 t_0} & & \lambda_n e^{-\lambda_n t_0} \\ \lambda_1 e^{-\lambda_1 t_1} & \lambda_2 e^{-\lambda_2 t_1} & & \lambda_n e^{-\lambda_n t_1} \\ \vdots & \vdots & \ddots & \vdots \\ \lambda_1 e^{-\lambda_1 t_m} & \lambda_2 e^{-\lambda_2 t_m} & & \lambda_n e^{-\lambda_n t_m} \end{vmatrix}, \quad (3)$$

$$\vec{x} = \begin{vmatrix} \overline{\nu}_{d,1} \\ \overline{\nu}_{d,2} \\ \vdots \\ \overline{\nu}_{d,n} \end{vmatrix}, \quad (4)$$

$$\vec{b} = \begin{vmatrix} \frac{\dot{n}_d(t_0)}{\varepsilon F_s} \\ \frac{\dot{n}_d(t_1)}{\varepsilon F_s} \\ \vdots \\ \frac{\dot{n}_d(t_m)}{\varepsilon F_s} \end{vmatrix}, \quad (5)$$

where the solution for the group yields with the given set of group constants is then calculated using the Scipy package's NonNegative Least Squares method.[15,16] The 2-norm condition number of A calculated using the singular value decomposition approach in NumPy is generally approximately 200.

An iterative process is used to modify the group decay constants. The iteration process goes through Eqs. (2) through (5) for every combination of values in L, an example of which is shown in Eq. (6) for a case with three decay constant nodes per DNP group:

$$L = \begin{vmatrix} (1-\mu)\lambda_1 & \lambda_1 & (1+\mu)\lambda_1 \\ (1-\mu)\lambda_2 & \lambda_2 & (1+\mu)\lambda_2 \\ \vdots & \vdots & \vdots \\ (1-\mu)\lambda_n & \lambda_n & (1+\mu)\lambda_n \end{vmatrix}. \quad (6)$$

The values of λ_g are linearly spaced from $(1-\mu)\lambda_g$ to $(1+\mu)\lambda_g$. The number of iterations for a given value of μ is equal to the number of decay constant nodes to the power of the number of groups. For six DNP groups, this means that to find the optimal set of decay constants, 729 iterations are required for three nodes, while 15 625 iterations would be required for five nodes.

Following an iteration for a given value of μ, the values of λ_g are set to the values that minimize chi-squared, as shown in Eq. (7):

$$\chi^2 = \sum_{j=1}^{m} \left(\frac{\dot{n}_{d,j} - \varepsilon F_s \sum_{g=1}^{n} \overline{\nu}_{d,g} \lambda_g e^{-\lambda_g t_j}}{\Delta \dot{n}_d(t_j)} \right)^2, \quad (7)$$

where

m = number of time nodes
n = number of precursor groups
$\dot{n}_{d,j}$ = delayed neutron count rate at time j
$\Delta \dot{n}_d(t_j)$ = uncertainty in delayed neutron count rate at time j.

Once a new solution is found that has a smaller value for chi-squared, the iteration goes back to the largest value of μ. For example, the values of μ in this work are set to 10%, 5%, 4%, 3%, 2%, 1%, and finally 0.5% to have decay constants resolved to within 0.5%. Starting with smaller values of μ means that the values of λ_g may take a long time to resolve or fail to find the best fit if the initial guess is far from the global chi-squared minimum. The convergence criteria used to stop is when the smallest value of μ no longer improves the fit.

The uncertainty in the delayed neutron count rate is discussed in Sec. II.E.

II.B. Group Spectrum Generation

Least-squares techniques are used for the yield and decay constants, but there is also a desire to have group spectra χ_g. This is referred to in this work as generating a spectral fit. In the past, the spectral fits were generated by allowing each isotope to contribute some fraction of its spectrum to its closest groups, sorted by group half-life[5,11,12] or based on nuclide half-life.[13,14] This work refers to such approaches as fractional fitting least squares. Alternatively, using an iterative least squares technique allows for a more optimal set of group spectra such that isotopes can contribute to more than two groups. This method also requires no individualized spectral data for the isotopes, yielding no potential error from erroneous spectral data within the fitting method. This method is referred to as iterative least squares in this work.

To determine the energy spectrum of neutrons emitted by each precursor group, the delayed neutron emission rate as a function of time and energy $\dot{n}_d(E,t)$ can be either collected from the ORIGEN output or generated from the IAEA database using Eq. (8):

$$\dot{n}_d(E,t) = \varepsilon \sum_{i=1}^{I} \chi_i(E) \lambda_i N_i(t) P_{n_i}, \quad (8)$$

where I is the total number of DNPs.

Once the two-dimensional (2D) set of values for $\dot{n}_d(E,t)$ is collected, the group spectra are generated using iterative least squares. This method iterates through each possible energy bin while solving the least squares problem for every time node, thus optimizing every j'th energy bin for all times. Equations (9) through (12) show the formulation for the solve, while Eq. (13) shows the residual solved for the nonlinear least squares solve[17,18]:

$$\dot{n}_d(E,t) \approx \varepsilon F_s \sum_{g=1}^{n} \chi_g(E) \lambda_g \overline{\nu}_{d,g} e^{-\lambda_g t}\,, \tag{9}$$

$$A = \begin{vmatrix} \lambda_1 \nu_{d,1} e^{-\lambda_1 t_0} & \lambda_2 \nu_{d,2} e^{-\lambda_2 t_0} & & \lambda_n \nu_{d,n} e^{-\lambda_n t_0} \\ \lambda_1 \nu_{d,1} e^{-\lambda_1 t_1} & \lambda_2 \nu_{d,2} e^{-\lambda_2 t_1} & & \lambda_n \nu_{d,n} e^{-\lambda_n t_1} \\ \vdots & \vdots & \ddots & \vdots \\ \lambda_1 \nu_{d,1} e^{-\lambda_1 t_m} & \lambda_2 \nu_{d,2} e^{-\lambda_2 t_m} & & \lambda_n \nu_{d,n} e^{-\lambda_n t_m} \end{vmatrix}, \tag{10}$$

$$\vec{x} = \begin{vmatrix} \chi_1(E_j) \\ \chi_2(E_j) \\ \vdots \\ \chi_n(E_j) \end{vmatrix}, \tag{11}$$

$$\vec{b} = \begin{vmatrix} \dfrac{\dot{n}_d(E_j,t_0)}{\varepsilon F_s} \\ \dfrac{\dot{n}_d(E_j,t_1)}{\varepsilon F_s} \\ \vdots \\ \dfrac{\dot{n}_d(E_j,t_m)}{\varepsilon F_s} \end{vmatrix}. \tag{12}$$

$$argmin_x \left|\left| \frac{Ax-b}{b} \right|\right|_2^2. \tag{13}$$

This form of the residual normalizes the problem such that the larger count rates at earlier times do not dominate the solve. Without this normalization, the problem would be dominated by the early timescales, leading to a poor fit at longer timescales where the count rate is much smaller.

II.C. Point Reactor Kinetics

Using the point reactor kinetics equations enables an understanding of how the group parameters will affect the reactor systems we are modeling. The time rate of change of neutrons in the system is given by

$$\frac{dn}{dt} = \frac{\rho-\beta}{\Lambda} n(t) + \sum_{g=1}^{6} \lambda_g C_g(t)\,, \tag{14}$$

where

ρ = reactivity

β = delayed neutron fraction

Λ = neutron generation time.

The time rate of change of the group g precursor concentration is given by

$$\frac{dC_g}{dt} = \frac{\beta_g}{\Lambda} n(t) - \lambda_g C_g(t)\,, \tag{15}$$

where β_g is the delayed neutron fraction of group g.

The initial conditions for Eqs. (14) and (15) are

$$\begin{aligned} n_0 &= 1 \\ C_{g_0} &= \beta_g n_0 \left(\lambda_g \Lambda\right)^{-1}. \end{aligned}$$

The β_g values are calculated using the group yields $\overline{\nu}_{d,g}$ and average neutron emission per fission event $\overline{\nu}$ as shown in Eq. (16):

$$\beta_g = \frac{\overline{\nu}_{d,g}}{\overline{\nu}}. \tag{16}$$

In this work, the equations were solved using the forward Euler method, shown in Eqs. (17) and (18):

$$n^{(m)} = n^{(m-1)} + \frac{dn^{(m-1)}}{dt}\Delta t\,, \tag{17}$$

$$C_g^{(m)} = C_g^{(m-1)} + \frac{dC_g^{(m-1)}}{dt}\Delta t\,, \tag{18}$$

The forward Euler method is used in this work because generating and providing results that demonstrate the differences yielded from each data set are simple using this approach. Because the purpose of the point reactor kinetics here is to demonstrate a general trend caused by differences between the DNP group parameters, a more advanced method would introduce more complexity than desired.

II.D. Tools and Modeling

To use the microscopic approach, it is necessary to simulate the irradiation of a sample. The tools used in this work are in-house Python scripts and SCALE 6.3, within which TRITON and ORIGEN were used for most of the analysis.[19] TRITON is a reactor physics and depletion sequence, and ORIGEN is a depletion and decay solver.[20] Specifically, the "T6-DEPL" TRITON sequence was used with the ENDF/B-VII.1 252-group neutron library. The T6-DEPL TRITON sequence enables TRITON to run with KENO-VI as neutron transport. These tools combined allow a reactor to be modeled, within which a sample can be irradiated. The composition of the sample can then be extracted and allowed to decay over time. POLARIS, which handles light water reactor lattice physics, was used for comparing the different DNP group parameters after the results were generated.

The primary model of interest in this work is Godiva, a uniform sphere of ^{235}U with a diameter of $6\frac{3}{4}$ in. and density of 19 g/cm^3.[21] Godiva is selected as the model of interest to replicate the experimental approach used by Keepin et al.[6] An additional model considered is a generic Westinghouse 17×17 pressurized water reactor (PWR), analyzed in Sec. III.E. The PWR model is used to understand the impact of the uncertainties and altered DNP group parameters. The TRITON input deck generated a Godiva geometry and imparted a 0.25-ms pulse irradiation with roughly 10^{16} fission events. The Godiva sphere does not deplete, but rather a 3-g sample within Godiva is irradiated, the same as in the Keepin et al. experiment.[6] The irradiation was then followed by a 330-s decay of the sample using logarithmically spaced time nodes to capture the short-lived DNPs' response in ORIGEN. This method replicated the one used by Keepin et al. so that the results could be directly compared.[6] In the Keepin et al. experiment, the data of interest used for analysis are the delayed neutron count over time.

Using data from the Godiva simulation and recently published experimental data, the delayed neutron count can be constructed. Equation (19) shows how the data come together to form the delayed neutron count $\dot{n}_d$:

$$\dot{n}_d(t) = \varepsilon \sum_{i=1}^{I} P_{n_i} \lambda_i N_i(t). \tag{19}$$

Equation (19) sums over all DNPs I, which can vary based on the dataset, and calculates the time-dependent delayed neutron count from each. This contribution from each DNP is then multiplied by the efficiency of the neutron detector ε. The detector efficiency term is set to 3.75×10^{-8} to scale the delayed neutron count profile to the results from Keepin et al.[6] Adjusting the efficiency term changes the delayed neutron count rate scaling but does not affect the generated group parameters themselves.

The concentration of each DNP in atoms $N_i(t)$ can be retrieved from the ORIGEN binary concentration file. The concentration of each DNP i can then be combined with the emission probability $P_{n,i}$ and decay constant λ_i for that DNP from the IAEA database to generate the neutron emission rate as a function of time. This can then be multiplied by the detector efficiency term ε to generate the delayed neutron count.

The delayed neutron count rate $\dot{n}_d(t)$ can be determined in two different ways using the previously described methodology. The first, called IAEA–ORIGEN in subsequent sections, is using ORIGEN to calculate $N_i(t)$ and IAEA emission probabilities P_{n_i} and decay constants λ_i to calculate $\dot{n}_d(t)$. The second, called Pure ORIGEN in subsequent sections, is by reading $\dot{n}_d(t)$ directly from the ORIGEN output, where ORIGEN uses a modified ENDF/B-VII.0 dataset for emission probabilities and decay constants. More specifically, the Pure ORIGEN delayed neutron count rate uses SCALE 6.2.4 neutron emission, which uses an embedded version of SOURCES4C, a code system that determines neutron production rates and spectra, combined with a modified ENDF/B-VII.0 dataset.[22] In some cases, IAEA–ORIGEN may require data to supplement the IAEA database. When this occurs, the IAEA–ORIGEN approach obtains data from the Evaluated Nuclear Structure Data File (ENSDF) and ENDF/B-VIII.0 to fill in gaps between the datasets.[2,23]

II.E. Uncertainty Tracking

An important consideration for the methods discussed are the uncertainties in the data used. The DNP group parameter uncertainties have contributions from decay constants, delayed neutron emission count rate, and fissions.[24] These uncertainties can be propagated to the DNP group parameters and spectra, which can then be propagated again to the models that use that data. In this work, these uncertainties are propagated through to the point reactor kinetics analysis.

The uncertainty in the delayed neutron emission count rate from ORIGEN can be determined based on Eq. (19), rewritten as follows:

$$\dot{n}_d(t) = \varepsilon \sum_{i=1}^{I} P_{n_i} \lambda_i N_{0_i} e^{-\lambda_i t},$$

by using Eqs. (20) through (23):

$$\frac{\partial \dot{n}_d(t)}{\partial P_{n_i}} = \lambda_i N_{0_i} e^{-\lambda_i t}\,, \tag{20}$$

$$\frac{\partial \dot{n}_d(t)}{\partial \lambda_i} = P_{n_i} N_{0_i}(1-\lambda_i t) e^{-\lambda_i t}\,, \tag{21}$$

$$\frac{\partial \dot{n}_d(t)}{\partial N_{0_i}} = P_{n_i} \lambda_i e^{-\lambda_i t}\,, \tag{22}$$

$$\Delta n_d^2(t) = \varepsilon \sum_{i=1}^{n} \left(\frac{\partial n_d(t)}{\partial P_{n_i}} \Delta P_{n_i}\right)^2 + \left(\frac{\partial n_d(t)}{\partial \lambda_i} \Delta \lambda_i\right)^2 + \left(\frac{\partial n_d(t)}{\partial N_{0_i}} \Delta N_{0_i}\right)^2 . \tag{23}$$

Equation (19) does not account for decay parents of the DNPs, instead treating the concentration of each as a decay over time from the initial concentration. The partial derivative is taken for each variable with uncertainty, which are the emission probability for DNP i P_{n_i}, the initial concentration of DNP i before measuring the delayed neutron count rate N_{0_i}, and the decay constant for DNP i λ_i. These partial derivatives are then used in the uncertainty calculation in the delayed neutron count from each individual DNP as shown in Eq. (23).

This uncertainty is then used in Eqs. (24) through (27) to calculate the uncertainty for the entire right-hand side of the least squares problem given in Eq. (2), repeated here:

$$A\vec{x} \approx \vec{b}\,.$$

The uncertainty in the emission probabilities ΔP_{n_i} comes from the IAEA data; the uncertainty in concentration ΔN_{0_i} comes from Sampler, a SCALE tool that stochastically computes and propagates uncertainties[20]; and the uncertainty in the decay constants $\Delta\lambda_i$ comes from the IAEA data for the ORIGEN delayed neutron count rate and is based on the mesh for the group parameters. Sampler is used with 500 samples, with perturbations in each non-metastable nuclide of cross sections, yields, and decay constants.

With the uncertainty in the delayed neutron count rate calculated, the uncertainty in the DNP group parameters is one step closer to being calculated. The next step is to propagate this uncertainty to the linear algebra equation that is used to find the DNP group parameters. Equation (24) is the right-hand side vector at a point in time m used when fitting the group constants:

$$\vec{b}_m = \frac{\dot{n}_d(t_m)}{\varepsilon F_s}. \tag{24}$$

Partial derivatives are taken with respect to the delayed neutron count rate and the number of fissions from Eq. (24), shown in Eqs. (25) and (26):

$$\frac{\partial \vec{b}_m}{\partial \dot{n}_d(t_m)} = \frac{1}{\varepsilon F_s}\,, \tag{25}$$

$$\frac{\partial \vec{b}_m}{\partial F_s} = -\frac{\dot{n}_d(t_m)}{\varepsilon F_s^2}. \tag{26}$$

These partial derivatives are then used to generate the uncertainty at that time, shown in Eq. (27):

$$\Delta \vec{b}_m = \frac{1}{\varepsilon}\sqrt{\left(\frac{\partial \vec{b}_m}{\partial \dot{n}_d(t_m)} \Delta n_d(t_m)\right)^2 + \left(\frac{\partial \vec{b}_m}{\partial F_s} \Delta F_s\right)^2}. \tag{27}$$

The uncertainty in the delayed neutron emission count rate from the group parameters can be found using Eq. (1) and the partial derivatives in Eqs. (28) and (29), yielding the result in Eq. (30):

$$\frac{\partial n_d}{\partial \bar{\nu}_{d,g}} = \lambda_g e^{-\lambda_g t}\,, \tag{28}$$

$$\frac{\partial n_d}{\partial \lambda_g} = \bar{\nu}_{d,g}(1-\lambda_g t) e^{-\lambda_g t}\,, \tag{29}$$

$$\Delta \dot{n}_d(t) = \varepsilon F_s \sqrt{\sum_{i=1}^{n} \left(\frac{\partial n_d}{\partial \bar{\nu}_{d,g}} \Delta \bar{\nu}_{d,g}\right)^2 + \left(\frac{\partial n_d}{\partial \lambda_g} \Delta \lambda_g\right)^2}. \tag{30}$$

The uncertainty in the group yield values $\Delta\bar{\nu}_{d,g}$ was calculated stochastically. The least squares problem used to solve for $\bar{\nu}_{d,g}$ was iterated upon with random variations within uncertainties for the various terms until the point at which a normal distribution formed and the standard deviation could be directly extracted. An example of this approach is shown Fig. 1, in which the sixth group yield is $(4.3 \pm 0.3) \times 10^{-4}$ delayed neutrons per fission.

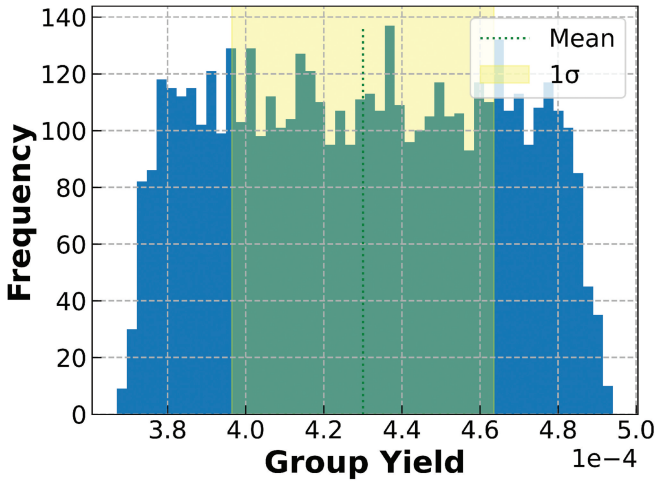

Fig. 1. Five thousand stochastic uncertainty simulations of the Keepin et al. sixth precursor group yield using a μ value of 0.5%.

Following the group parameter generation is the point reactor kinetics uncertainties that use the forward Euler method. The decay constant uncertainty comes from the group parameter generation; the initial uncertainties in both the number of neutrons at the current time $\Delta n^{(m)}$ and the number of precursors in the i'th group $\Delta C_g^{(m)}$ are zero; and the group and total delayed neutron fraction uncertainties $\Delta\beta_i$ and $\Delta\beta$, respectively, are given in Eqs. (31) and (32):

$$\Delta\beta_i = \sqrt{\left(\frac{1}{\overline{\nu}}\Delta\overline{\nu}_{d,g}\right)^2 + \left(\frac{\overline{\nu}_{d,g}}{\overline{\nu}^2}\Delta\overline{\nu}\right)^2}, \tag{31}$$

$$\Delta\beta = \sqrt{\left(\sum_{i=1}^{n}\Delta\beta_g^2\right)}. \tag{32}$$

The uncertainty in $n^{(m)}$ from Eq. (17), rewritten with the fully expanded derivative in Eq. (33), is given in Eq. (39), with the components given in Eqs. (34) through (38). In these equations, Δt is the time step used in the forward Euler method:

$$\begin{aligned} n^{(m)} &= n^{(m-1)} + \tfrac{\rho-\beta}{\Lambda}n^{(m-1)}\Delta t \\ &+ \sum_{i=1}^{n}\left(\lambda_g C_g^{(m-1)}\Delta t + \tfrac{\beta_g}{\Lambda}n^{(m-1)}\lambda_g\Delta t^2 - \lambda_g^2 C_g^{(m-1)}\Delta t^2\right), \end{aligned} \tag{33}$$

where the partial derivatives are taken with respect to the previous time step's number of neutrons $n^{(m-1)}$, decay constant for each group λ_g, delayed neutron fraction β, delayed neutron fraction for each group β_g, and the previous time step's precursor concentration for each group $C_g^{(m-1)}$. The partial derivatives are given as

$$\frac{\partial n^{(m)}}{\partial n^{(m-1)}} = 1 + \frac{\rho-\beta}{\Lambda}\Delta t + \sum_{i=1}^{n}\frac{\beta_g}{\Lambda}\lambda_g\Delta t^2, \tag{34}$$

$$\begin{aligned} \frac{\partial n^{(m)}}{\partial \lambda_g} &= C_g^{(m-1)}\Delta t + \frac{\beta_g}{\Lambda}n^{(m-1)}\Delta t^2 \\ &- 2\lambda_g C_g^{(m-1)}\Delta t^2, \end{aligned} \tag{35}$$

$$\frac{\partial n^{(m)}}{\partial \beta} = \frac{-n^{(m-1)}\Delta t}{\Lambda}, \tag{36}$$

$$\frac{\partial n^{(m)}}{\partial \beta_g} = \frac{n^{(m-1)}\lambda_g\Delta t^2}{\Lambda}, \tag{37}$$

$$\frac{\partial n^{(m)}}{\partial C_g^{(m-1)}} = \lambda_g\Delta t - \lambda_g^2\Delta t^2. \tag{38}$$

The partial derivatives are then used to calculate the uncertainty in the number of neutrons at iteration m:

$$\begin{aligned} \left(\Delta n^{(m)}\right)^2 = &\sum_{i=1}^{n}\left(\frac{\partial n(t)}{\partial n^{(m-1)}}\Delta n^{(m-1)}\right)^2 + \left(\frac{\partial n(t)}{\partial \lambda_g}\Delta\lambda_g\right)^2 \\ &+ \left(\frac{\partial n(t)}{\partial \beta}\Delta\beta\right)^2 + \left(\frac{\partial n(t)}{\partial \beta_g}\Delta\beta_g\right)^2 \\ &+ \left(\frac{\partial n(t)}{\partial C_g^{(m-1)}}\Delta C_g^{(m-1)}\right)^2. \end{aligned} \tag{39}$$

The uncertainty in C_g from Eq. (18), rewritten with the fully expanded derivative in Eq. (40), is given by Eq. (45), incorporating the components given by Eqs. (41) through (44):

$$C_g^{(m)} = C_g^{(m-1)} + \frac{\beta_g}{\Lambda}n^{(m-1)}\Delta t - \lambda_g\Delta t C_g^{(m-1)}, \tag{40}$$

where the partial derivatives are taken with respect to the same variables as the equation for the number of neutrons:

$$\frac{\partial C_g^{(m)}}{\partial C_g^{(m-1)}} = 1 - \lambda_g \Delta t\,, \tag{41}$$

$$\frac{\partial C_g^{(m)}}{\partial \beta_g} = \frac{n^{(m-1)}\Delta t}{\Lambda}\,, \tag{42}$$

$$\frac{\partial C_g^{(m)}}{\partial n^{(m-1)}} = \frac{\beta_g \Delta t}{\Lambda}\,, \tag{43}$$

$$\frac{\partial C_g^{(m)}}{\partial \lambda_g} = -C_g^{(m-1)}\Delta t. \tag{44}$$

The partial derivatives are then used to calculate the uncertainty in each precursor group concentration at iteration m:

$$\left(\Delta C_g^{(m)}\right)^2 = \sum_{i=1}^{n}\left(\frac{\partial C_g^{(m)}}{\partial n^{(m-1)}}\Delta n^{(m-1)}\right)^2 + \left(\frac{\partial C_g^{(m)}}{\partial \lambda_g}\Delta\lambda_g\right)^2 + \left(\frac{\partial C_g^{(m)}}{\partial \beta_g}\Delta\beta_g\right)^2 + \left(\frac{\partial C_g^{(m)}}{\partial C_g^{(m-1)}}\Delta C_g^{(m-1)}\right)^2. \tag{45}$$

Finally, the uncertainty of group spectra constructed using the iterative linear least squares procedure is shown in Eq. (46):

$$\dot{n_d}(E,t) = \dot{n_d}(t)\sum_g \chi_g(E). \tag{46}$$

This uncertainty is fairly straightforward to calculate because the delayed neutron count term $\dot{n_d}(t)$ comes from the six group parameters for which the uncertainty is given in Eq. (30). The uncertainty for the energy-dependent neutron emission count rate is shown in Eq. (47), where the uncertainty in the spectra $\Delta\chi_g(E)$ is calculated stochastically, in the same manner as the group yield uncertainties:

$$\Delta n_d^2(E,t) = \left(\Delta\dot{n_d}(t)\sum_g \chi_g(E)\right)^2 + \left(\left(\dot{n_d}(t)\right)^2\sum_g\left(\Delta\chi_g(E)\right)^2\right). \tag{47}$$

III. RESULTS AND ANALYSIS

III.A. ORIGEN Data Compared with IAEA Data

Because the group parameters are fit to the delayed neutron count data, it is important to understand how the data compare. The two different datasets compared are the previously discussed IAEA–ORIGEN and the Pure ORIGEN datasets. For analysis of the delayed neutron emission count rate, the three components that can change from the datasets are the time-dependent compositions term, the decay constants term, and the emission probabilities term, all of which were first presented in Eq. (19).

The composition as a function of time depends on the incident fission neutron energy, the fission yield, the decay constant of the target isotope, and that same data for any isotopes that decay into the target isotope. In this work, the ORIGEN- and IAEA-based data comparisons use the compositions generated by KENO-VI and decayed in ORIGEN.

We can conduct a sensitivity study of the decay constants λ and emission probabilities (or branching fractions) P_n by comparing the results of the Pure ORIGEN dataset simulated in ORIGEN with the IAEA dataset in ORIGEN. Specifically, we can adjust the data such that only decay constants, only emission probabilities, or both are swapped from the Pure ORIGEN dataset values to the IAEA dataset values.

Figure 2 shows the net count rate for the Pure ORIGEN and for the IAEA–ORIGEN data sets in which the percent difference of the Pure ORIGEN to the IAEA–ORIGEN count rate appears to be close. The percent difference between the count rates initially starts at ~1.5%, peaks at a 14% difference shortly thereafter, and then drops again. Figures 3, 4, and 5 provide more information on the short-lived and longer-lived isotopes that lead to this percent difference. These figures are generated by comparing count rate differences from decay constants, emission probabilities, and both at the same time. The plots show the difference of the Pure ORIGEN count rate with the IAEA–ORIGEN count rate subtracted away. The negative count rate differences are represented as dashed lines, while the positive count rate differences are solid lines. The nuclides are selected by tracking whichever nuclides have the largest absolute difference at each time step, as the shorter-lived nuclides will have a smaller absolute difference as they decay away. Figure 3 shows that the peak decay constant difference causes around 1.2 million counts per second, while the difference drops rapidly during later times. The count rate difference is larger because of the emission probability difference than the decay constant difference. This can be seen by comparing the differences in Figs. 3 and 4 at various times.

Table I lists the isotopes that have the most significant effect on the decay constant and emission probability data differences. Figures 4 and 5 show the impact these nuclides have on the delayed neutron count rate. From Table I, it can be seen that the emission probabilities affect the majority of the nuclides with the largest differences. These emission probability differences drive differences in the net yield as well. Table II shows the net yields from various data sets and shows that changing the decay constants does not largely impact the net yield. However, changing emission probabilities has a nonnegligible impact of approximately 200 pcm. This is because the net yield measures the total number of delayed neutrons, which means the time at which they are emitted is less important than the net number that are emitted.

Figure 6 shows how the initial spectrum of the ORIGEN output compares to the IAEA–ORIGEN spectrum, with uncertainties, immediately after irradiation. Although these results account for only one time step, the spectral differences become smaller over time, as shown in Fig. 7. While Fig. 6 shows the energy spectra at a single time step, Fig. 7 shows the difference of the average of the energy spectra at each time step.

Figure 7 shows that the IAEA–ORIGEN data yield a larger average energy than the Pure ORIGEN data at every time step, which is demonstrated in Fig. 6. This discrepancy between the energy spectra shortly after irradiation aligns with the previously discussed results. Additionally, because the main differences occur in the first 2 s, the problematic isotopes can be determined directly. The results shown in Figs. 3, 4, and 5 indicate that those isotopes that differ most significantly within the first 2 s are ^{91}Br, ^{85}As, ^{86}As, ^{137}I, and ^{138}I.

III.B. Six Group Parameters

The DNP six groups can be calculated using the generated delayed neutron count rate data and iterative least squares method. Recall from Sec. II that a detector efficiency ε of 3.75E-8 is used in all results to reflect the experimental results from Keepin et al.[6]

Table II lists the net yield variance observed between the IAEA data and ORIGEN library data calculated by summing the group yields. Additionally, net yields from other works are shown for fast ^{235}U irradiation. Overall, it can be seen that the calculated yields generally agree with the range of values from the literature. The top four of the table shows that there is a large difference between the yields based on the emission probability data. This is because a shift in the decay constant data minimally affects the net yield.

Tables III and V contain the group half-life and yield parameters, which were identified using the iterative least squares approach and the group parameters taken from Brady and England, referenced here since they are the parameters used in ENDF, and from Keepin et al.[6,12] The results from Keepin et al. are directly compared with this work since their experimental setup is replicated. The results from Brady and England, which use the microscopic approach, use preliminary data from ENDF/B-VI.[29] Although the methods are similar to the methods in this work, differences can be expected with the Brady and England results because of the difference in the data used. The uncertainties for the group parameters are given in Tables IV and VI. An interesting note is that the IAEA group parameters are all smaller than all the other fits, which means that the delayed neutrons will

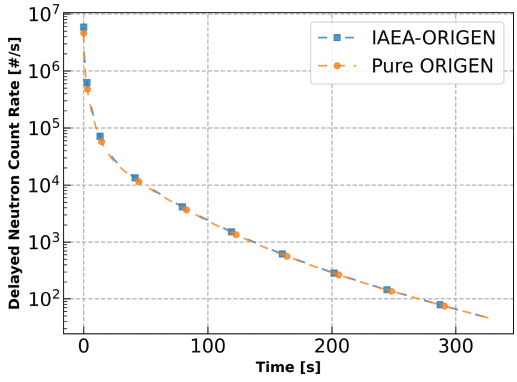

(a) Pure ORIGEN and IAEA–ORIGEN count rate over time

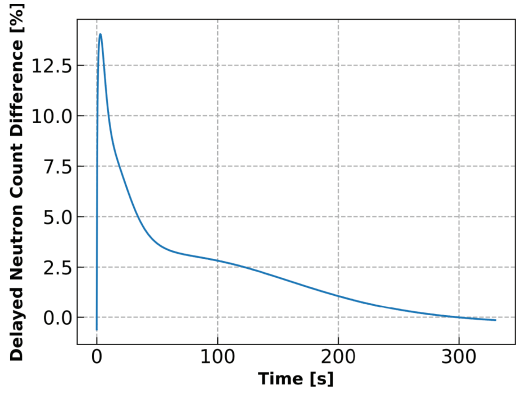

(b) Pure ORIGEN and IAEA–ORIGEN count rate difference over time normalized by the IAEA–ORIGEN count rate

Fig. 2. Comparison of delayed neutron count rate for Pure ORIGEN and IAEA–ORIGEN data after fast-pulse irradiation of ^{235}U.

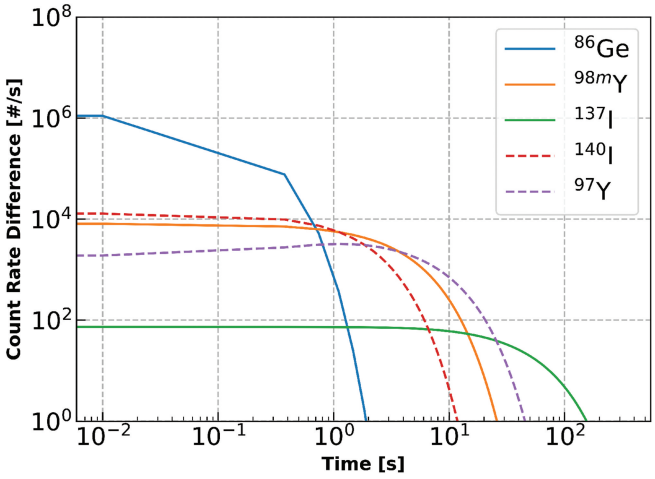

Fig. 3. The decay constant–based difference between Pure ORIGEN count rates and Pure ORIGEN with IAEA decay constants for ^{235}U fast-pulse irradiation over time. The dotted lines represent a negative count rate difference, meaning the IAEA decay constants increase the count rate for those nuclides.

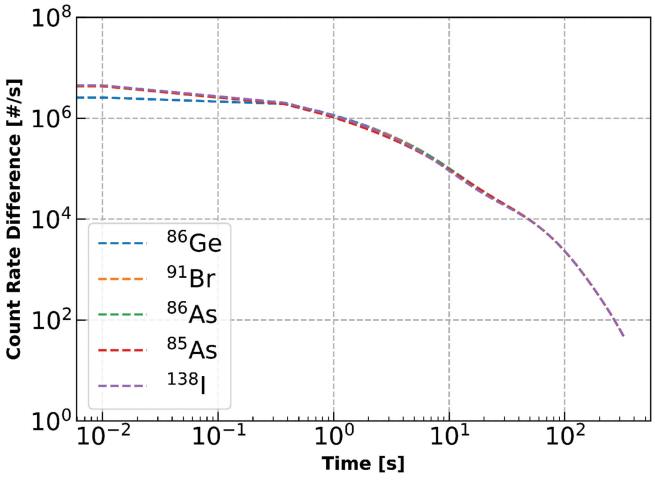

Fig. 4. The emission probability (i.e., branching fraction)–based difference between the Pure ORIGEN count rates and Pure ORIGEN with IAEA decay constants for ^{235}U fast-pulse irradiation over time. The dotted lines represent a negative count rate difference, meaning the IAEA emission probabilities increase the count rate for those nuclides.

overall be emitted more rapidly compared to the other fits.

For the group yields, the IAEA fit showed greater weight on the longer-lived groups, which is noticeable when comparing the longest- and shortest-lived group yields. A comparison of the fits is shown in Fig. 8; this comparison indicates that the DNP group parameters in the current work are similar to other group parameters. The comparison also reveals discrepancies among the

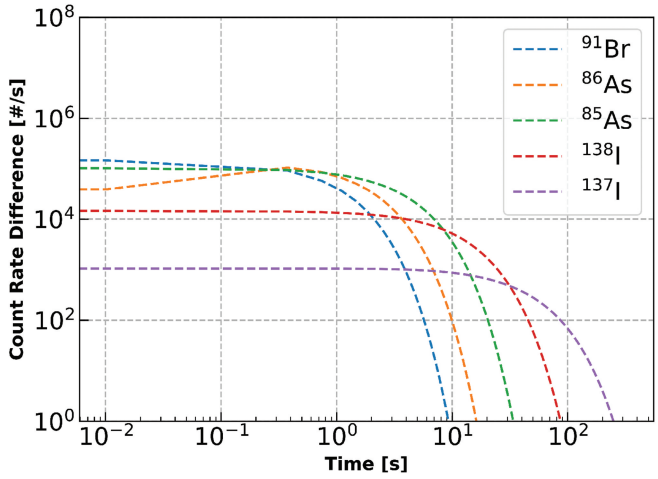

Fig. 5. The combined decay constant and emission probability–based difference between Pure ORIGEN count rates and IAEA–ORIGEN count rates for ^{235}U fast-pulse irradiation over time. The dotted lines represent a negative count rate difference, meaning the combined IAEA decay constants and emission probabilities increase the count rate for those nuclides.

other referenced fits, although all of the fits shown are for the same fissile isotope and fast energy spectrum.

The discrepancies could be the result of differences in energy spectra causing fission, uncertainty in the number of fission events, uncertainty in the experimental data collected by Keepin et al. (which were fitted), or uncertainty in the nuclear data used in the codes in this work and in Brady and England's work.

III.C. Six Group Spectra

Using the six group parameters generated, as well as the energy-dependent count rate from ORIGEN and the constructed data from the IAEA database, the spectral profiles associated with each group can be generated, as shown in Eq. (9). Figure 9 compares the discrepancy between the historical fractional fitting approach and the proposed iterative least squares approach. The iterative least squares provides a visually better fit than that of the fractional fitting method. This is shown specifically at 330 s, where the longest-lived groups dominate the spectra.

III.D. Point Reactor Kinetics Reactivity Insertion

To observe the effect of altering the group parameters, the response to a reactivity step insertion can be modeled using point reactor kinetics. In this problem, we use the following parameters: a neutron generation time

TABLE I

Decay and Emission Data for Isotopes with the Largest Count Rate Discrepancies

Isotope	λ_{IAEA} (s−1)	λ_{ORIGEN} (s−1)	$\Delta\lambda$ (s−1)	P_{IAEA}	P_{ORIGEN}	ΔP
^{91}Br	1.27	1.28	0.01	0.304	0.109	0.195
^{85}As	0.343	0.343	0.00	0.625	0.22	0.405
^{86}As	0.734	0.733	0.001	0.345	0.105	0.240
^{137}I	0.028	0.028	0.00	0.076	0.072	0.004
^{138}I	0.111	0.111	0.00	0.053	0.026	0.027
^{86}Ge	3.12	7.30	4.18	0.45	0.22	0.23
^{98m}Y	0.299	0.347	0.048	0.034	0.034	0.00
^{140}I	1.17	0.806	0.364	0.079	0.22	0.141
^{97}Y	0.185	0.185	0.00	5.8E-4	0.003	0.00242

TABLE II

Net Delayed Neutron Yields from Various Sources of Data for Fast ^{235}U*

λ	P_n	Yield
IAEA	IAEA	0.0191
ORIGEN	IAEA	0.0193
IAEA	ORIGEN	0.0172
ORIGEN	ORIGEN	0.0172
Keepin et al.[6]	Keepin et al.[6]	0.0165
Brady and England[12]	Brady and England[12]	0.0206
Tuttle[26]	Tuttle[26]	0.0167
ENDF/B-V[27]	ENDF/B-V[27]	0.0167
England et al.[28]	England et al.[28]	0.0198
England and Rider[29]	England and Rider[29]	0.0206
ENDF/B-VII.0[30]	ENDF/B-VII.0[30]	0.0162
JEFF-2.2[31]	JEFF-2.2[31]	0.0191
JEFF-3.1.1[32]	JEFF-3.1.1[32]	0.0170

*Partially recreated from Refs. [12] and [25].

of 0.1 μ s, an average number of total neutrons per fission of 2.6, and the DNP group parameters from Sec. III.B. Figure 10 shows the neutron density response to a reactivity step insertion into a reactor with these parameters.

Figure 10 shows that the Keepin et al. response was slightly lower than that of the current work.[6] The responses began closely aligned and diverged further apart as the effect of the DNPs becomes more significant. In the later times, the IAEA–ORIGEN neutron density was slightly lower than the Pure ORIGEN neutron density. This is because the group parameters of Pure ORIGEN have higher yield values for five and six groups, the yield values of which dominate during the early times. This effect was counteracted slightly by the slightly longer lives of five and six groups that Pure ORIGEN also has, but the net effect was still an increased response compared with that of the IAEA–ORIGEN group parameters. Following this logic, the Keepin et al. group parameters have small yields for five and six groups while also having fairly long half-lives for each group.

III.E. Westinghouse 17×17 PWR

Additional macroscopic analysis was conducted using SCALE/Polaris. SCALE/Polaris is a tool used to perform 2D lattice physics that provides six group kinetics parameters as an output. These outputs are importance weighted, nuclide integrated, and assembly homogenized. Because these kinetics parameters are used by other codes to perform transient analyses, it is important to determine the difference using the default kinetic parameters used as an

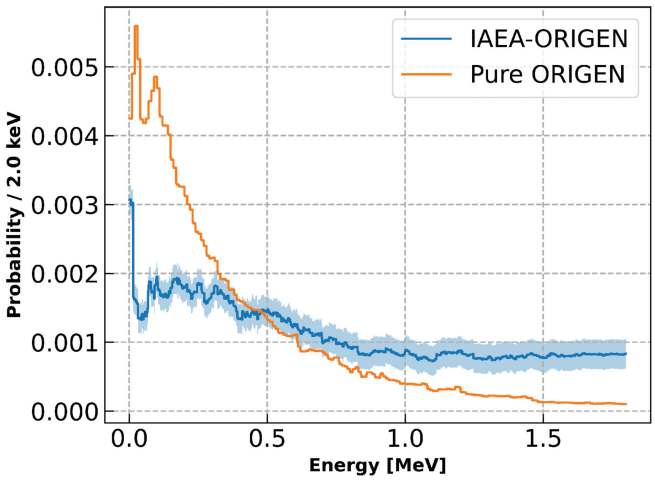

Fig. 6. Normalized difference in emission spectra of Pure ORIGEN and IAEA–ORIGEN for ^{235}U fast-pulse irradiation at 0 s with uncertainty tracked for the IAEA–ORIGEN results.

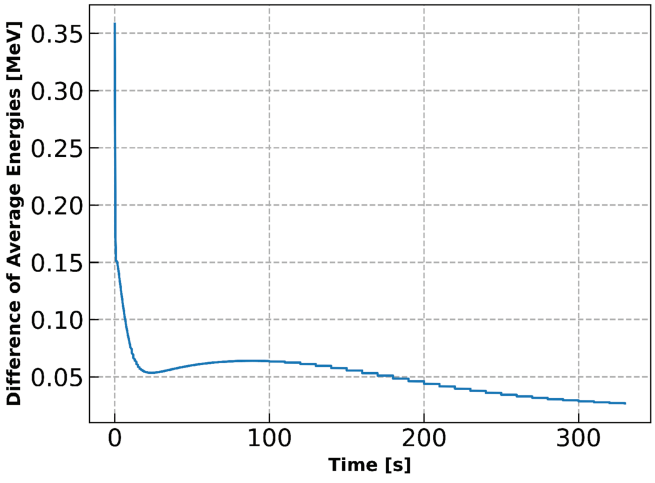

Fig. 7. Difference in average delayed neutron energy of Pure ORIGEN and IAEA–ORIGEN for ^{235}U fast-pulse irradiation over time where Pure ORIGEN is subtracted from IAEA–ORIGEN.

input compared with the six group parameters generated in this work.

For this analysis, only the fast spectrum kinetics parameters were altered for ^{235}U. This adjustment was performed to provide a conservative estimate for the magnitude of difference, which can be expected because of the heavily thermal spectrum.

The default values used for the kinetic parameter inputs are those from Keepin et al.[6] The IAEA and Pure ORIGEN six group parameters presented in this work were then used. The resulting kinetics parameter outputs for each set of group parameters were compared, with the absolute percent differences shown in Fig. 11.

These absolute percent differences from the Keepin et al. data show that the largest difference in IAEA yield and half-life values was observed in the third precursor group; the greatest difference in those values for Pure ORIGEN was observed in the sixth precursor group. This result corresponds directly to the differences in the six group parameters shown in Tables III and V. In particular, the IAEA-ORIGEN third precursor group has a yield of 0.670, which is almost double the Pure ORIGEN third precursor group yield of 0.244. Even though fast fission of ^{235}U in the Westinghouse PWR is not the primary mode of fission, the large difference in the group yield data still leads to a difference of approximately 8% in the net group 3 yields.

IV. CONCLUSIONS AND FUTURE WORK

This work demonstrates generation of DNP group parameters from a simulated irradiation combined with data from the IAEA and from ORIGEN.[1] These group parameters use recent experimental data and propagated uncertainties to investigate the effects on reactor

TABLE III

Six Group Half-Lives Given in Seconds

Fit	T_1	T_2	T_3	T_4	T_5	T_6
Brady and England[12]	52.1	21.2	5.74	2.29	0.816	0.243
Keepin et al.[6]	54.5	21.8	6.00	2.23	0.496	0.179
IAEA–ORIGEN	49.0	19.2	3.64	1.28	0.320	0.098
Pure ORIGEN	51.3	20.7	6.04	2.19	0.505	0.115

TABLE IV

Six Group Half-Lives' Uncertainties Given in Seconds

Fit	ΔT_1	ΔT_2	ΔT_3	ΔT_4	ΔT_5	ΔT_6
Keepin et al.[6]	0.94	0.54	0.17	0.06	0.03	0.02
IAEA–ORIGEN	0.245	0.096	0.018	0.006	0.002	0.001
Pure ORIGEN	0.256	0.104	0.030	0.011	0.003	0.001

TABLE V

Six Group Yields in Delayed Neutrons per Fission Multiplied by 100

Fit	$\overline{\nu}_{d,1}$	$\overline{\nu}_{d,2}$	$\overline{\nu}_{d,3}$	$\overline{\nu}_{d,4}$	$\overline{\nu}_{d,5}$	$\overline{\nu}_{d,6}$
Brady and England[12]	0.072	0.372	0.355	0.797	0.327	0.137
Keepin et al.[6]	0.063	0.351	0.310	0.672	0.211	0.043
IAEA–ORIGEN	0.083	0.350	0.670	0.566	0.187	0.054
Pure ORIGEN	0.071	0.308	0.244	0.711	0.300	0.091

TABLE VI

Six Group Yields' Uncertainties in Delayed Neutrons per Fission Multiplied by 100

Fit	$\Delta\overline{\nu}_{d,1}$	$\Delta\overline{\nu}_{d,2}$	$\Delta\overline{\nu}_{d,3}$	$\Delta\overline{\nu}_{d,4}$	$\Delta\overline{\nu}_{d,5}$	$\Delta\overline{\nu}_{d,6}$
Keepin et al.[6]	0.005	0.011	0.028	0.023	0.015	0.005
IAEA–ORIGEN	0.009	0.009	0.008	0.003	0.003	0.001
Pure ORIGEN	0.014	0.018	0.012	0.007	0.002	0.001

behavior. The results showed that some of the DNP data used in ORIGEN differ with the data from the IAEA database.

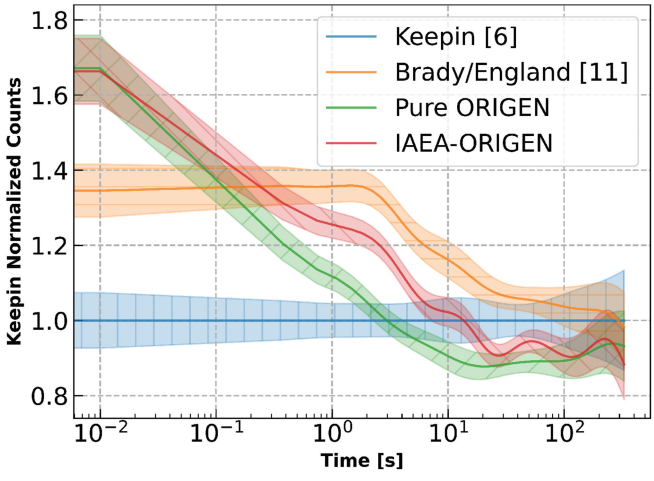

Fig. 8. A comparison of the different fast fission irradiation DNP six group parameters of ^{235}U normalized to the Keepin et al. six group count rate with uncertainties.[6]

Specifically, a few particular nuclides have large differences between the IAEA database and in ORIGEN. The nuclides with the largest impact on the delayed neutron count rate following fast spectrum pulse irradiation of ^{235}U from data discrepancies include ^{91}Br, ^{85}As, ^{86}As, ^{137}I, ^{138}I, ^{86}Ge, ^{98m}Y, ^{140}I, and ^{97}Y. These discrepancies result in a 200 pcm difference in the total delayed neutron yield, as well as differences in the rate at which the delayed neutrons are emitted. The two sets of group parameters generated from these differing data in a point reactor kinetics model showed that the resulting neutron density responses are similar over a relatively short time period after large reactivity insertions. Discrepancies among the data between SOURCES4C and ENDF are currently being dealt with by relying more on ENDF and less on SOURCES4C where possible in SCALE.

The group spectrum generation was also investigated in this work. The proposed method, which allows each DNP to contribute to every DNP group, showed promising results, providing a better fit than the fractional fitting method. The iterative least squares method proposed is more computationally expensive, but it is worthwhile

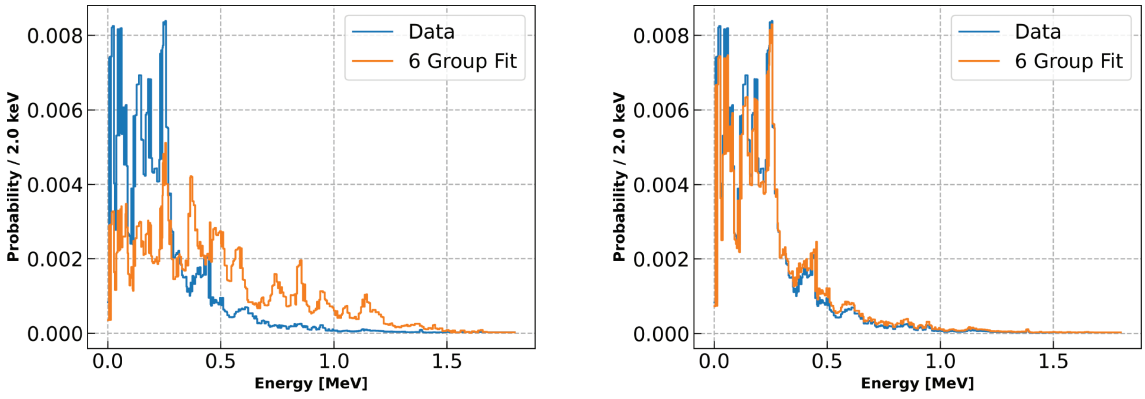

(a) Fractional fitting (b) Iterative least squares

Fig. 9. Comparison of data with normalized IAEA–ORIGEN six group spectra for ^{235}U pulse irradiation at 330 s.

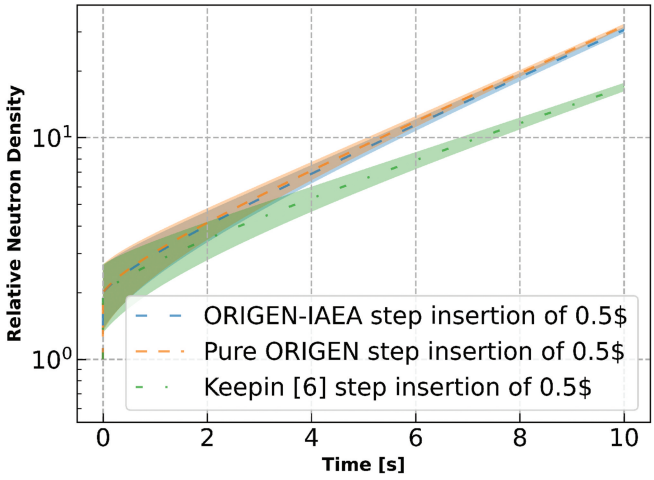

Fig. 10. Point reactor kinetic neutron density response to reactivity step insertion for different six group parameters.

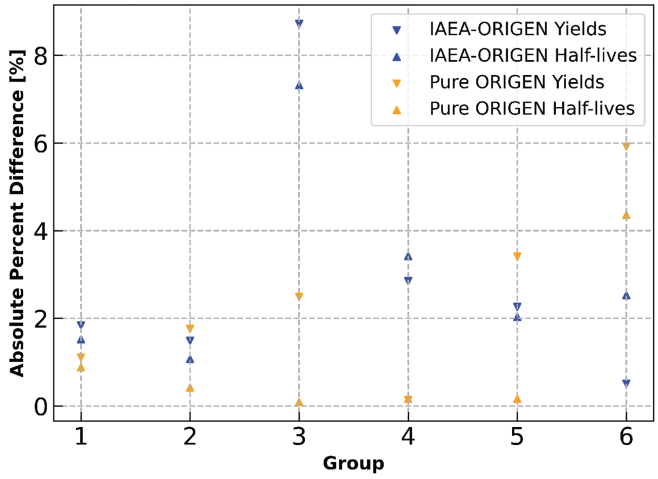

Fig. 11. The absolute percent difference of IAEA and Pure ORIGEN six group parameters to the Keepin et al. parameters of fast spectrum ^{235}U in a Westinghouse 17 × 17 fuel assembly.

provided the group spectra do not need to be regenerated frequently.

There are many different possible extensions that can further this work. Updates could be made to the group parameters by implementing updated data and propagating uncertainty. The group spectra could also be updated with uncertainty propagation and methods for fitting optimal group spectra. A more thorough analysis of various group parameter fitting methods for yields and spectra could include using nonlinear least squares or other least squares methods, calculating uncertainty when the decay constant mesh is refined to the furthest extent possible, and determining whether other methods would alter how many groups are needed for a fit within a given margin.

Analysis of additional data sources, such as the Joint Evaluated Fission and Fusion library or using the General Description of Fission Observables (GEF) model code, could similarly identify additional isotopes causing discrepancies.[33] Also of interest are comparisons with kinetics benchmarks by investigating other energy spectra, fissile nuclides, and kinetics methodologies.[34–36] A tool such as Moltres can incorporate these group parameters to simulate three-dimensional kinetics benchmark problems.[37–40]

Acknowledgments

Thanks are due to Ugur Mertyurek for reviewing this paper. Additional thanks are due to the University of Illinois Department of Nuclear, Plasma, and Radiological Engineering and the members of the Advanced Reactors and Fuel Cycles group for their support and suggestions in developing this work.

Funding

This manuscript has been authored by UT-Battelle, LLC under contract DE-AC05-00OR22725 with the US Department of Energy (DOE). The US government retains and the publisher, by accepting the article for publication, acknowledges that the US government retains a nonexclusive, paid-up, irrevocable, worldwide license to publish or reproduce the published form of this manuscript, or allow others to do so, for US government purposes. DOE will provide public access to these results of federally sponsored research in accordance with the DOE Public Access Plan (http://energy.gov/downloads/doe-public-access-plan). This material is based upon work supported under an Integrated University Program Graduate Fellowship. The authors are grateful for this generous support. Any opinions, findings, conclusions or recommendations expressed in this publication are those of the author(s) and do not necessarily reflect the views of the Department of Energy Office of Nuclear Energy.

Disclosure Statement

No potential conflict of interest was reported by the author(s).

Author Contributions

CRediT: **Luke Seifert:** Data curation, Formal analysis, Investigation, Methodology, Project administration, Software, Visualization, Writing – original draft, Writing – review & editing; **Benjamin Betzler:** Conceptualization, Project administration, Resources, Supervision; **William Wieselquist:** Investigation, Project administration, Supervision, Writing – review & editing; **Matthew Jessee:** Project administration, Supervision, Writing – review & editing; **Madicken Munk:** Supervision, Writing – review & editing; **Kathryn Huff:** Supervision, Writing – review & editing.

ORCID

Luke Seifert http://orcid.org/0000-0002-9860-4341
Benjamin Betzler http://orcid.org/0000-0001-8425-9711
William Wieselquist http://orcid.org/0000-0002-2211-7395
Matthew Jessee http://orcid.org/0000-0003-2954-4995
Madicken Munk http://orcid.org/0000-0003-0117-5366
Kathryn Huff http://orcid.org/0000-0002-7075-6802

References

1. P. DIMITRIOU et al., "Development of a Reference Database for Beta-Delayed Neutron Emission," *Nucl. Data Sheets*, **173**, 144 (2021); https://doi.org/10.1016/j.nds.2021.04.006.
2. D. BROWN et al., "ENDF/B-VIII.0: The 8th Major Release of the Nuclear Reaction Data Library with CIELO-Project Cross Sections, New Standards and Thermal Scattering Data," *Nucl. Data Sheets*, **148**, 1 (2018); https://doi.org/10.1016/j.nds.2018.02.001.
3. T. PARISH et al., "Status of Six-Group Delayed Neutron Data and Relationships Between Delayed Neutron Parameters from the Macroscopic and Microscopic Approaches," *Nucl. Sci. Eng.*, **131**, *2*, 208 (1999); https://doi.org/10.13182/NSE99-A2029.
4. M. CHADWICK et al., "ENDF/B-VII.0: Next Generation Evaluated Nuclear Data Library for Nuclear Science and Technology," *Nucl. Data Sheets*, **107**, *12*, 2931 (2006); https://doi.org/10.1016/j.nds.2006.11.001.
5. M. C. BRADY, "Evaluation and Application of Delayed Neutron Precursor Data," PhD Thesis, Texas A&M University (1988).
6. G. KEEPIN, T. WIMETT, and R. ZEIGLER, "Delayed Neutrons from Fissionable Isotopes of Uranium, Plutonium and Thorium," *J. Nucl. Energy*, **6**, *1*, IN2 (1957); https://doi.org/10.1016/0891-3919(57)90178-X.
7. D. J. HUGHES et al., "Delayed Neutrons from Fission of U^{235}," *Phys. Rev.*, **73**, 111 (1948); https://doi.org/10.1103/PhysRev.73.111.
8. D. J. LOAIZA et al., "Measurements of Absolute Delayed Neutron Yield and Group Constants in the Fast Fission of ^{235}U and ^{237}Np," *Nucl. Sci. Eng.*, **128**, *3*, 270 (1998); https://doi.org/10.13182/NSE98-A1955.
9. D. J. LOAIZA and F. E. HASKIN, "Dominant Delayed Neutron Precursors to Model Reactivity Predictions for Multiple Fissioning Nuclides," *Nucl. Sci. Eng.*, **134**, *1*, 22 (2000); https://doi.org/10.13182/NSE00-A2097.
10. P. LECONTE et al., "New Delayed Neutron Group Constants and Covariances for LWR Core Applications, Combining Summation Calculations and Integral Experiments," *Ann. Nucl. Energy*, **139**, 107250 (2020); https://doi.org/10.1016/j.anucene.2019.107250.
11. D. SAPHIER et al., "Evaluated Delayed Neutron Spectra and Their Importance in Reactor Calculations," *Nucl. Sci. Eng.*, **62**, *4*, 660 (1977); https://doi.org/10.13182/NSE77-A15209.
12. M. C. BRADY and T. R. ENGLAND, "Delayed Neutron Data and Group Parameters for 43 Fissioning Systems," *Nucl. Sci. Eng.*, **103**, *2*, 129 (1989); https://doi.org/10.13182/NSE103-129.
13. G. RUDSTAM, "Six-Group Representation of the Energy Spectra of Delayed Neutrons from Fission," *Nucl. Sci. Eng.*, **80**, *2*, 238 (1982); https://doi.org/10.13182/NSE82-A21428.
14. T. R. ENGLAND et al., "Aggregate Delayed Neutron Intensities and Spectra Using Augmented ENDF/

B-V Precursor Data," *Nucl. Sci. Eng.*, **85**, *2*, 139 (1983); https://doi.org/10.13182/NSE83-A27422.

15. C. L. LAWSON and R. J. HANSON, *Solving Least Squares Problems*, SIAM (1995).
16. R. BRO and S. DE JONG, "A Fast Non-Negativity-Constrained Least Squares Algorithm," *J. Chemom.*, **11**, *5*, 393 (1997); https://doi.org/10.1002/(SICI)1099-128X(199709/10)11:5<393::AID-CEM483>3.0.CO;2-L.
17. P. VIRTANEN et al. SciPy 1.0 Contributors, "SciPy 1.0: Fundamental Algorithms for Scientific Computing in Python," *Nat. Methods*, **17**, 261 (2020); https://doi.org/10.1038/s41592-019-0686-2.
18. M. A. BRANCH, T. F. COLEMAN, and Y. LI, "A Subspace, Interior, and Conjugate Gradient Method for Large-Scale Bound-Constrained Minimization Problems," *SIAM J. Sci. Comput.*, **21**, *1*, 1 (1999); https://doi.org/10.1137/S1064827595289108.
19. L. SEIFERT, "GitHub Repository with Scripts," https://doi.org/10.5281/zenodo.14888551 (2025).
20. W. WIESELQUIST and R. A. LEFEBVRE, "SCALE 6.3.1 User Manual," ORNL/TM-SCALE-6.3.1, Oak Ridge National Laboratory (2023); https://www.osti.gov/biblio/1959594.
21. R. E. PETERSON and G. A. NEWBY, "An Unreflected U-235 Critical Assembly," *Nucl. Sci. Eng.*, **1**, 112 (1956); https://api.semanticscholar.org/CorpusID:123304404.
22. W. B. WILSON et al., "SOURCES: A Code for Calculating (α,n), Spontaneous Fission, and Delayed Neutron Sources and Spectra," *Radiat. Prot. Dosim.*, **115**, *1–4*, 117 (2005); https://doi.org/10.1093/rpd/nci260.
23. J. K. TULI et al., "Evaluated Nuclear Structure Data File," *A Manual for Preparation of Data Sets*, Brookhaven National Laboratory, National Nuclear Data Center (2001).
24. M. I. RADAIDEH, W. A. WIESELQUIST, and T. KOZLOWSKI, "A New Framework for Sampling-Based Uncertainty Quantification of the Six-Group Reactor Kinetic Parameters," *Ann. Nucl. Energy*, **127**, 1 (2019); https://doi.org/10.1016/j.anucene.2018.11.043.
25. T. HUYNH and C. JOUANNE, "Calculation of Delayed Neutron Yields for Various Libraries," *Nucl. Data Sheets*, **118**, 476 (2014); https://doi.org/10.1016/j.nds.2014.04.111.
26. R. TUTTLE, "Delayed-Neutron Yields in Nuclear Fission," *Proc. 2nd Consultants' Mtg. Delayed Neutron Properties*, Vienna, Austria, March 26–30, 1979, p. 29, International Atomic Energy Agency (1979).
27. R. KINSEY et al., "ENDF/B Summary Documentation," Brookhaven National Laboratory (1979).
28. W. B. WILSON and T. R. ENGLAND, "Delayed Neutron Study Using ENDF/B-VI Basic Nuclear Data," *Prog. Nucl. Energy*, **41**, *1–4*, 71 (2002); https://doi.org/10.1016/S0149-1970(02)00006-9.
29. T. R. ENGLAND and B. F. RIDER, "Status of Fission Yield Evaluations," Los Alamos National Laboratory (1983); https://www.osti.gov/biblio/5509379.
30. M. CHADWICK et al., "ENDF/B-VII. 0: Next Generation Evaluated Nuclear Data Library for Nuclear Science and Technology," *Nucl. Data Sheets*, **107**, *12*, 2931 (2006); https://doi.org/10.1016/j.nds.2006.11.001.
31. "The JEF-2.2 Nuclear Data Library," NEA Data Bank (2000).
32. A. SANTAMARINA et al., "The JEFF-3.1.1 Nuclear Data Library – JEFF Report 22, Organisation for Economic Co-operation and Development, Nuclear Energy Agency (2009).
33. K.-H. SCHMIDT et al., "General Description of Fission Observables: GEF Model Code," *Nucl. Data Sheets*, **131**, 107 (2016); https://doi.org/10.1016/j.nds.2015.12.009.
34. A. E. ABOANBER, "Generalized and Stability Rational Functions for Dynamic Systems of Reactor Kinetics," *Int. J. Nucl. Energy*, **2013**, *1*, 903904 (2013); https://doi.org/10.1155/2013/903904.
35. B. D. GANAPOL, "A Refined Way of Solving Reactor Point Kinetics Equations for Imposed Reactivity Insertions," *Nucl. Technol. Radiat. Prot.*, **24**, *3*, 157 (2009); https://doi.org/10.2298/NTRP0903157G.
36. J. NÓBREGA da, "A New Solution of the Point Kinetics Equations," *Nucl. Sci. Eng.*, **46**, *3*, 366 (1971); https://doi.org/10.13182/NSE71-A22373.
37. A. LINDSAY et al., "Introduction to Moltres: An Application for Simulation of Molten Salt Reactors," *Ann. Nucl. Energy*, **114**, 530 (2018); https://doi.org/10.1016/j.anucene.2017.12.025.
38. S. M. PARK, "Advancements in Moltres for Time-Dependent Multiphysics Molten Salt Reactor Modeling," PhD Dissertation, University of Illinois Urbana-Champaign (2025).
39. S. KLIEM et al. "A Benchmark for Coupled 3D Neutron Kinetics/Thermohydraulics System Codes – Main Steam Header Break in A NPP with VVER-440 Reactor," *Proc. Mathematics and Computation, Reactor Physics and Environmental Analysis in Nuclear Applications*, Madrid, Spain, September 27–30, 1999.
40. J. B. BRIGGS and J. GULLIFORD, "An Overview of the International Reactor Physics Experiment Evaluation Project," *Nucl. Sci. Eng.*, **178**, *3*, 269 (2014); https://doi.org/10.13182/NSE14-27.